

ABOLLE-OKOYEAGU, C.J., FATUKASI, O., DROUBI, G. and REUBEN, R.L. 2024. Quantitative analysis of the Hsu-Nielsen source through advanced measurement and simulation techniques. *Journal of physics: conference series* [online], 2805: proceedings of the 8th International conference on mechanical, aeronautical and automotive engineering 2024 (ICMAA 2024), 02-04 February 2024, Penang, Malaysia, article 012013. Available from: <https://doi.org/10.1088/1742-6596/2805/1/012013>

Quantitative analysis of the Hsu-Nielsen source through advanced measurement and simulation techniques.

ABOLLE-OKOYEAGU, C.J., FATUKASI, O., DROUBI, G. and REUBEN, R.L.

2024

Content from this work may be used under the terms of the Creative Commons Attribution 4.0 licence. Any further distribution of this work must maintain attribution to the author(s) and the title of the work, journal citation and DOI.
The file associated with this output contains the article as published in the conference proceedings and the slide presentation presented at the conference, which have been combined into a single file on this repository.

PAPER • OPEN ACCESS

Quantitative Analysis of the Hsu-Nielsen Source through Advanced Measurement and Simulation Techniques

To cite this article: C J Abolle-Okoyeagu *et al* 2024 *J. Phys.: Conf. Ser.* **2805** 012013

View the [article online](#) for updates and enhancements.

You may also like

- [Fatigue crack sizing in rail steel using crack closure-induced acoustic emission waves](#)
Dan Li, Kevin Sze Chiang Kuang and Chan Ghee Koh
- [Non-velocity Based Analysis of Passive Ultrasonic Signal for Source Location Detection in Composite Plates: A Pilot Study](#)
Z M Hafizi, J Epaarachchi, C K E Nizwan et al.
- [Feasibility study of using smart aggregates as embedded acoustic emission sensors for health monitoring of concrete structures](#)
Weijie Li, Qingzhao Kong, Siu Chun Michael Ho et al.

PRIME
PACIFIC RIM MEETING
ON ELECTROCHEMICAL
AND SOLID STATE SCIENCE
HONOLULU, HI
October 6-11, 2024

Joint International Meeting of
The Electrochemical Society of Japan (ECSJ)
The Korean Electrochemical Society (KECS)
The Electrochemical Society (ECS)

Early Registration Deadline:
September 3, 2024

**MAKE YOUR PLANS
NOW!**

Quantitative Analysis of the Hsu-Nielsen Source through Advanced Measurement and Simulation Techniques

C J Abolle-Okoyeagu*, Oluseyi Fatukasi¹, Ghazi Droubi¹ and R L Reuben²

¹ Robert Gordon University, Garthdee House, Garthdee, Aberdeen AB10 7AQ, UK

² Heriot Watt University Edinburgh, Boundary Road North, Edinburgh EH14 4AS, UK

*corresponding author's e-mail: j.abolle-okoyeagu@rgu.ac.uk

Abstract. This paper presents the results from conducting a series of experiments with a Hsu-Nielsen Source, accompanied by corresponding numerical simulations on a solid block. The aim being to illustrate a Finite Element Analysis (FEA) approach for simulating Acoustic Emission (AE) wave propagation in a Hsu-Nielsen Source, by employing virtual sensors to enhance existing AE research methodologies. The objective was to examine and establish the actual unload rate derived from Pencil Lead Breaks (PLBs) by comparing results from simulations and experimental trials. These experiments and simulations were conducted using a solid cylindrical steel block, capturing the propagating Acoustic AE waves from both sources over a two-second span. When comparing the experimental data with the simulation results, it is evident that replicating the structure of an impulsive AE source is feasible for brief durations. Furthermore, both the experimental and simulated signals on the steel cylinder displayed comparable patterns in the initial 25-30 μ s. The methodology presented in this study demonstrates the effectiveness of Finite Element Analysis (FEA) in precisely identifying the specific modes present in AE wave propagation, including the actual unload rates affecting the AE signals recorded.

1. Introduction

Acoustic Emission (AE) is characterized by stress waves in the high-frequency range (0.1 to 1MHz), generated by the abrupt discharge of mechanical energy often associated with structural degradation. The technique of Acoustic Emission Testing (AET) employs these waves as they propagate to detect irregularities in structures and processes and machinery [1], [2], [3], [4]. Over time, AET has gained recognition as a viable Non-Destructive Testing (NDT) technique due to its efficiency in assessing structural health with minimal monitoring points and its ability to use wave propagation characteristics for fault detection [5], [6] [7], [8] Unlike other NDT methods like ultrasonics or radiography which depend on external imaging to identify flaws, AET is unique as it detects degradative processes by analysing energy inherently generated within the material itself [9],[10].

Calibration of AE systems is essential for ensuring the accuracy and reliability of measurements which are critical for assessing the integrity and safety of various structures and materials [11], [12]. [13], [14]. The AE calibration test object is a crucial tool in the maintenance and verification of AE testing equipment. By providing a controlled source of acoustic emissions, it allows for the standardization and validation of AE systems, ensuring that they produce consistent and accurate results for structural health monitoring. With ongoing advancements in AE technology, calibration test objects



continue to evolve, offering higher precision and adaptability to various testing scenarios [14], [15], [16].

The Hsu-Nielsen Source which is generally known as the Pencil Lead Break (PLB) is the standard AE calibration technique, it serves as a typical method for replicating and characterizing sensors in AE applications. This process entails exerting pressure on a test structure's surface with a pencil lead and inducing a bending moment at a specific angle. The force exerted results in a localized deformation of the test surface which is subsequently released upon the breaking of the lead. It provides a consistent benchmark for AE systems, verifies sensor sensitivity and enables reproducibility of results across different AE systems and tests [17], [18]

Finite Element Analysis (FEA) is a computational technique designed to predict and analyse the response of a structure subjected to various external forces. This is accomplished by obtaining approximate solutions to intricate mathematical problems in which the dependent variables satisfy a differential equation within a well-defined range of independent variables. [19]. FEA has increasingly become a popular method for simulating the propagation of elastic waves that are indicative of AE events [20], [21], [22]. In contrast to ultrasonic Non-Destructive Testing (NDT) waves, the propagation of Acoustic Emission (AE) waves is considerably more complex, even in simple homogeneous materials like flat plates. This complexity stems from the nature of AE waves, which are typically produced by relatively uncontrolled events, as opposed to the controlled wave generation in ultrasonic NDT achieved through ultrasonic transducers. [23].

A significant portion of research using FEA for simulating AE has concentrated on characterizing wave propagation [24] [25], [26] yet there has been minimal exploration of the connection between the source input and the sensor output. Moreover, even within the studies on propagation, there has been scant attention given to the topic of attenuation in a manner that holds practical value. Hence, this work aims to ascertain what insights can be garnered regarding the characteristics of an AE source through the data collected by sensors arrayed along a solid steel cylinder. Attaining this objective necessitates the coupling of simulations with a series of concurrent experiments, which are strategically designed to exert maximum control over both the source and the boundaries of the test subject.

2. Materials and methods

The selected test object is a steel cylinder, with its configuration as a reference object deliberately chosen due to its prior assessment in previous studies. [27].

2.1. Experimental technique

In the experiments, we utilized a standard Hsu-Neilson source, PAC-1220A pre-amplifiers, and PAC Micro U80D-93 broad band piezoelectric AE sensors to generate AE and capture the ensuing wave signals. The preamplifiers were configured with a gain of 40dB.

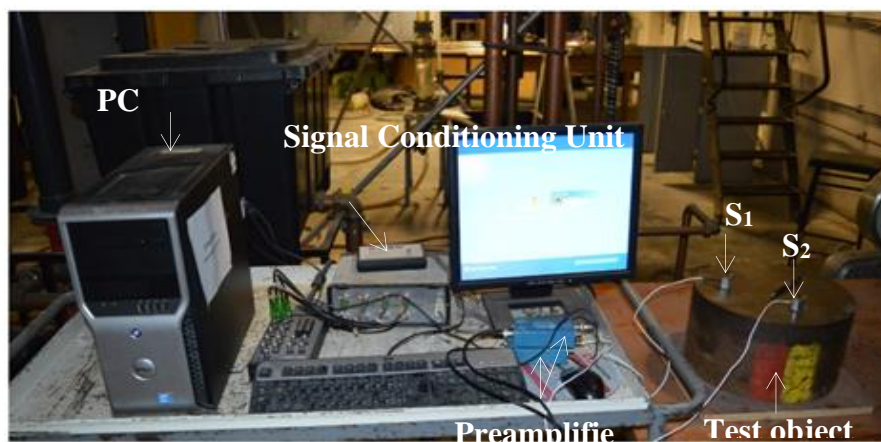


Figure 1. AE experimental setup

The test object, A solid steel cylinder, measuring approximately 0.17 meters in length and 0.31 mm in diameter, was utilized, positioned upright on one of its circular faces. The opposite circular face served as the test surface. Two broadband sensors were affixed to this test surface, each placed 0.0785 meters from the edge, while the AE source was positioned centrally (figure 1). For the initial part of the experiment, both sensors remained attached to the cylinder, and 20 lead breaks were recorded without any removal or reattachment of the sensors. Subsequently, an additional set of 20 lead break experiment was conducted, during which the sensors were removed and then reattached after each break. Despite Sensor 1 (S1) serving as the trigger sensor, there was negligible or no difference in the signal arrival times at the two sensors. To ensure consistency in detecting the signal arrival time, and thresholding technique [28] was utilized using the first sensor as the trigger.

2.2. Finite element simulation

FEA replicating the aforementioned experimental setups were conducted using the dynamic explicit solver in ABAQUS (provided by Dassault Systemes, Vélizy-Villacoublay, France). For the test model, A 3D elastic steel cylinder, with pressure unloading akin to a Pencil Lead Break (PLB) situated at the centre of the top surface, was modelled with the bottom surface being completely constrained. The data were collected from a point within the Finite Element (FE) model, positioned at 0.0785 meters from the left-hand edge of the top surface.

The selected rise times were within the range documented in existing literature, and the outcomes of the various unload rates can be found in [29] The force and surface area used (Table 1) are estimated values derived from the PLB experiment.

The explicit dynamic module of ABAQUS software was used to capture the transient stress patterns emerging from rapid pressure variations and for signal processing, the MatLab software was utilized.

The material properties used were those of steel (table 1).

Table 1. FE simulation parameters

Young Modulus	210GPa
Density	7800kg/m ³
Area	0.003m ² .
Force	100N
Element Type	C3D8R Elements
Mesh Size	0.01mm
Boundary Condition	Fixed

Six different unload rates (2×10^{-8} s, 5.11×10^{-7} s, 1×10^{-6} s, 1.5×10^{-6} s, 1.98×10^{-6} s, 2.47×10^{-6} s) were studied. The unload rates were set to approximate the time it would take a fracture traveling at the speed of sound to traverse the diameter of a 0.5mm pencil lead. This was done so that the simulated responses could be aligned and compared with the observed responses of Pencil Lead Breaks (PLBs) as documented in [28]. The simulation results were captured as time series data, beginning as soon as the virtual sensor detects the activation of the source. This recording starts at the point when the source was applied to the solid cylinder and continued until the end of the simulation, which occurred 0.02s after the source was applied.

4. Results and discussion

4.1. Experimental results

Figure 2 shows comprehensive recording of a typical raw Acoustic Emission (AE) time series produced by a Hsu-Nielsen source, as captured by both sensors on the solid cylinder. It is evident from the figure

that the peak amplitude is attained rapidly and is subsequently followed by a more prolonged ring-down phase, which persists for the full length of the recording (10ms).

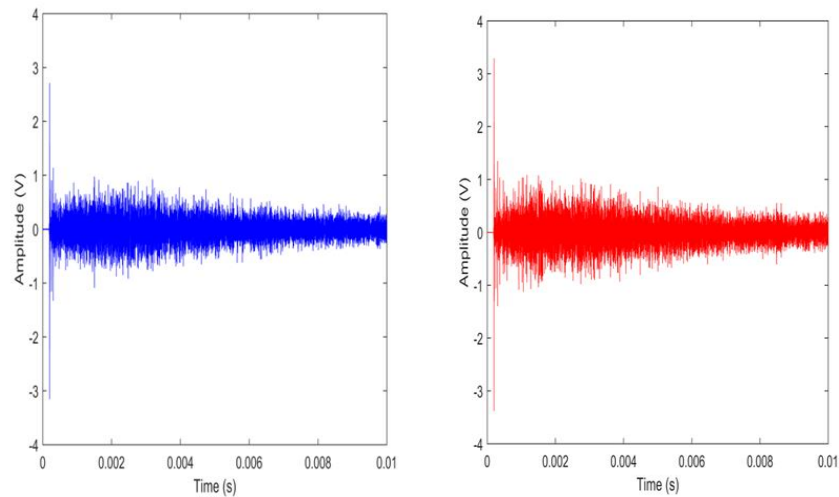


Figure 2: Standard raw AE signal acquired by a Hsu-Nielsen source, recorded at both sensors on the steel cylinder.

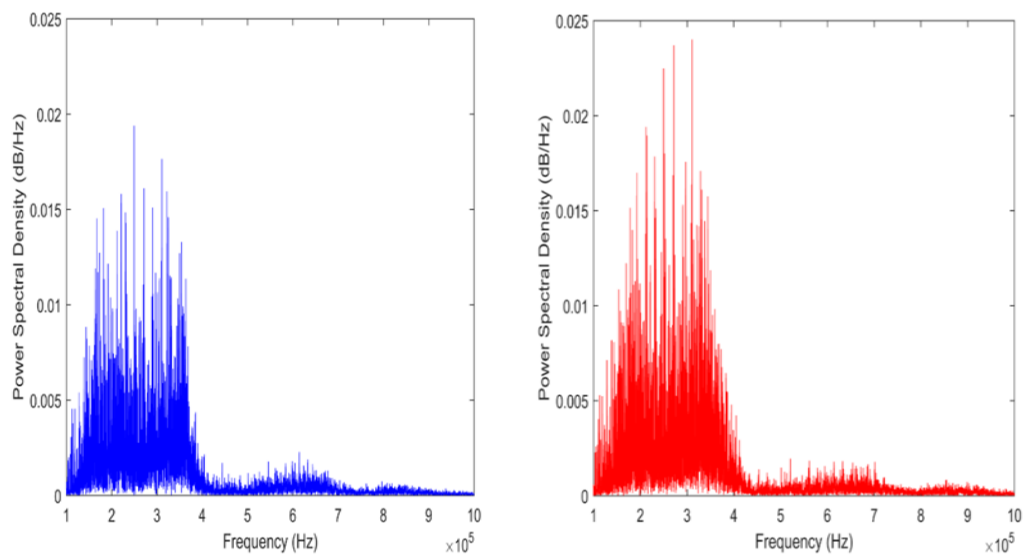


Figure 3: Power spectra of entire time series shown in figure 2 for both sensors on the steel cylinder.

4.2. Simulation results

Figure 4 shows the time series simulated at the two sensors, capturing the initial 10ms for the examined unload rate (1×10^{-6} s). The wave at the first and second sensors are shown in blue and red respectively. The signals suggest that as the wave disperses and undergoes reflection, there is a gradual decrease in its amplitude over time. Additionally, an increase in the unload rate corresponds to a diminishing wave amplitude.

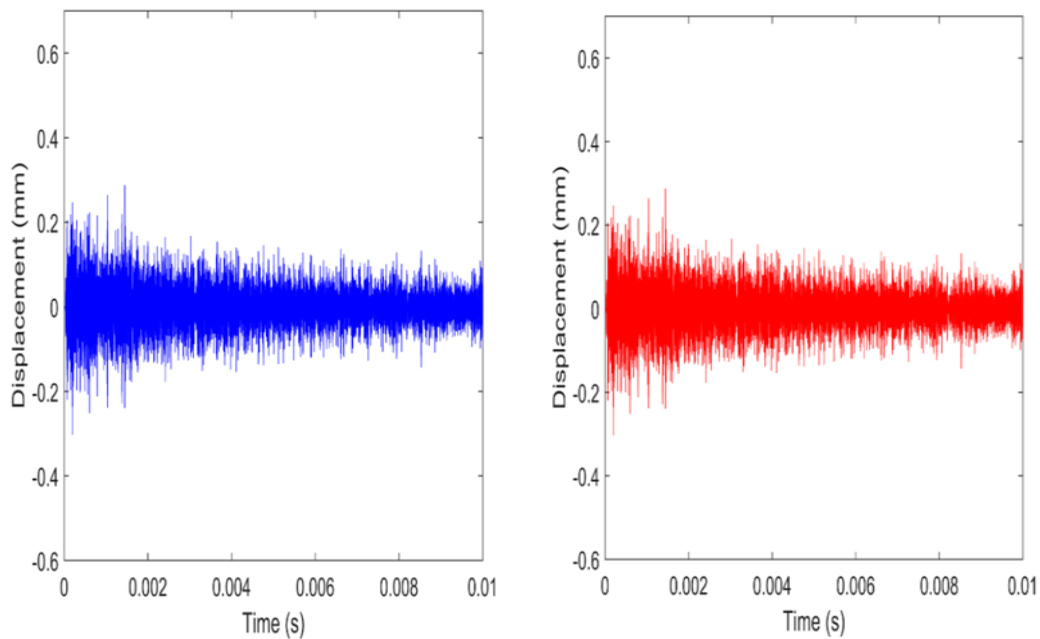


Figure 4: Raw AE signal of displacement at both virtual sensors the steel cylinder unloading at 1×10^6 s.

Figure 5 shows the frequency spectra at the first sensor for the time series depicted in Figure 4. There is a noticeable immediate frequency cut-off at 400 kHz, which is attributed to the effective sampling rate determined by the time steps in the simulation.

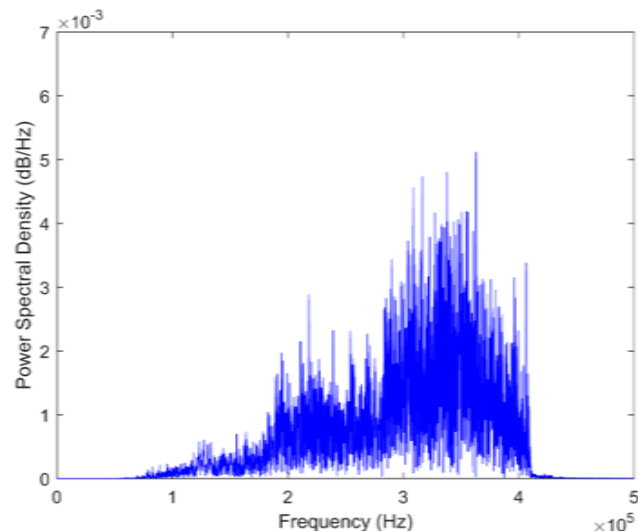


Figure 5: AE frequency spectra for time series in Figure 4 unloading at 1×10^6 s.

In the simulation, the velocities of the two waves can be approximately calculated to be around 3000ms^{-1} and 1250ms^{-1} , assuming both are traveling across the surface from the source to the sensor. The former speed aligns well with the speed of Rayleigh waves, whereas the latter does not match the speed of any known pure modal wave. For the experimental records, given the similar positioning of the sensors, analysing the energy and the power spectrum can help assess the uniformity of the 20 PLBs and the consistent response of the two sensors. To further examine the spectra presented in Figure 5,

three new frequency bands were identified (upon inspection); below 200 kHz (low frequency, LF), 200-500 kHz (medium frequency, MF), and above 500 kHz (high frequency, HF). This categorization results in three power values: P_{LF} , P_{MF} , and P_{HF} , and three indicators as proportions of the total power:

$$f_i = \frac{P_i}{P_{LF} + P_{MF} + P_{HF}}$$

Table 2 provides a summarized view of the total power frequency structure for both the experimental and simulated data on the solid cylinder at sensor position S1. The experimental figures are derived from the average power values of 20 experimental measurements. In a similar manner, proportions for the simulations at S1 and for each unload rate were computed. Since sensors S1 and S2 are essentially at the same distance, their total power frequency structures are identical, though there are slight variations in the experimental data. For simplicity in referencing, condition codes have been assigned to the simulations.

Table 2. Total power and fraction distribution across the frequency bands for both experiments and simulations.

Condition	Code	f_{LF}	f_{MF}	f_{HF}	P_{tot}
Expt, sensor 1	ES ₁ F	0.39	0.43	0.18	3.23
Expt, sensor 2	ES ₂	0.38	0.49	0.13	4.07
1 st Simulated unload rate	Sim1S ₁ R	0.39	0.57	0.04	0.03
2 nd Simulated unload rate	Sim2S ₁ R	0.39	0.57	0.04	0.42
3 rd Simulated unload rate	Sim3S ₁ R	0.41	0.56	0.04	0.75
4 th Simulated unload rate	Sim4S ₁ R	0.43	0.53	0.03	0.10
5 th Simulated unload rate	Sim5S ₁ R	0.47	0.50	0.03	1.14
6 th Simulated unload rate	Sim6S ₁ R	0.51	0.46	0.03	1.12

Figure 6 compares the power spectral content at the first sensor, contrasting the measured (E) and simulated (Sim) results for the shorter time series.

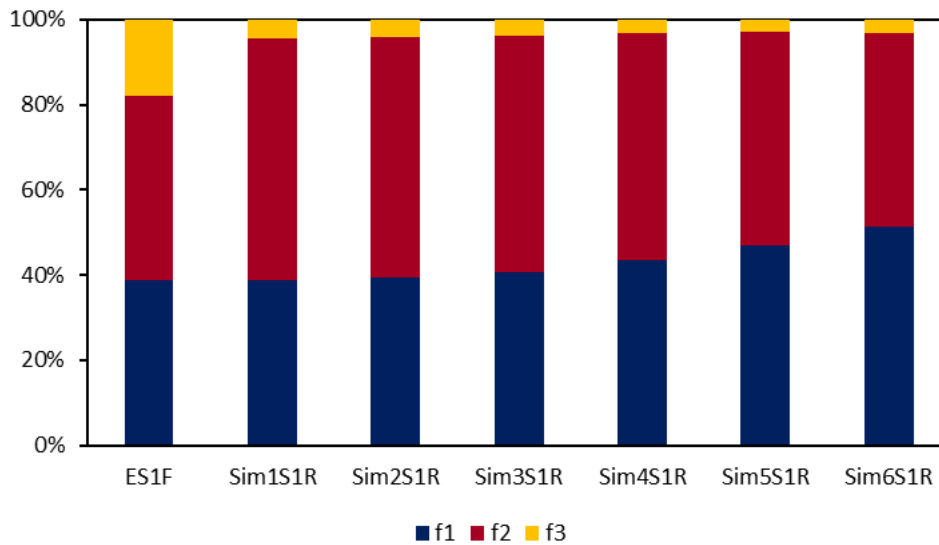


Figure 6: Comparison of experimental and simulated power content at first sensor

Observations indicate that, with extended unload durations, there's a noticeable shift towards lower frequencies, aligning with the anticipated increase in frequencies as one approaches a step unload. Additionally, the fact that the experimental spectra generally display lower low frequency content compared to the simulations suggests that the highest unload rate tested in this study is the most appropriate. However, it's important to note that the reduced high frequency (HF) content in the simulations is partially due to the time-step employed, making it an artefact of the simulation process.

Figure 7 illustrates the changes in power content between the low and medium frequency bands, revealing a consistent decrease in the ratio of LF to MF as the unload rate increases. By excluding HF band in this analysis, it appears that lower unload rates, specifically in the range of 4 to 5, may more accurately reflect the observed phenomena.

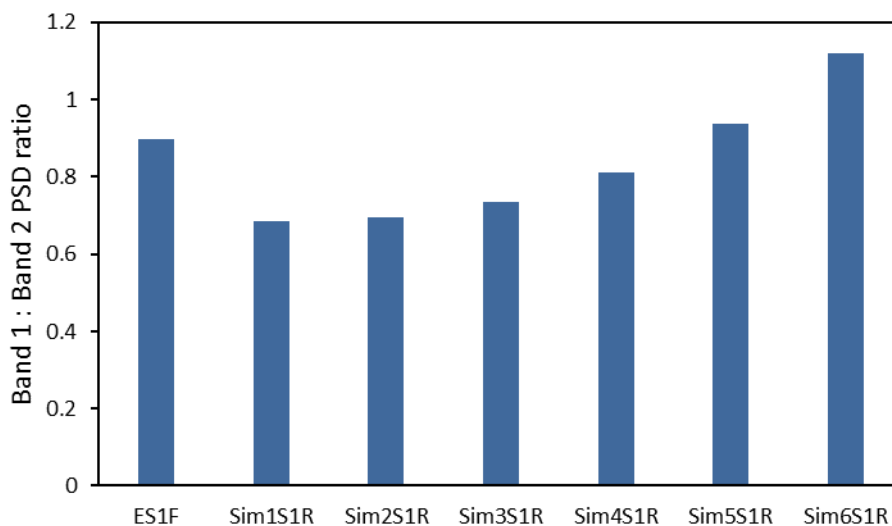


Figure 7. Comparison of experimental and simulated low frequency power ratio

Figure 8 illustrates how the unload rate impacts the total simulated power content of the signal at sensor S1. It is evident that the total power accelerates substantially from the fastest rate, while the slope

gradually declines as the unload rates decrease. Additionally, it's worth noting that the total power at the highest unload rate is approximately sixty times lesser than that at the lowest rate.

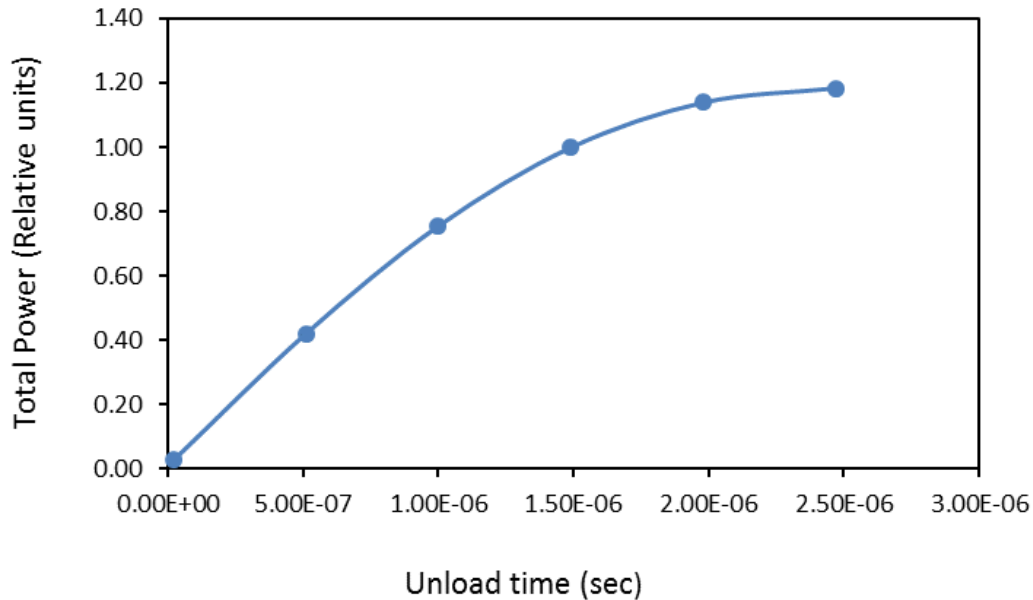


Figure 8: Simulation power vs unloading rate.

In both the experimental and simulation scenarios, the AE detected in the block was rapidly affected by reflections from the block's edges and bottom surface. In the first 25-30 μ s, the experiments and simulation on the steel cylinder showed comparable patterns. However, beyond this period, the actual measurements yielded clearer signals. This increased clearness is due to energy losses caused by reflections, an aspect that the simulations did not incorporate. This observation suggests that, in their current form, the simulations are useful for interpreting the structure of the source primarily during the initial phases of arrival in the case of small objects.

5. Conclusion

The comparison between pencil lead break experiments and equivalent simulations on a steel block suggests that while initial signals in both cases are similar, measured signals become clearer over time due to energy losses from reflections not accounted for in simulations. Despite artificial constraints in simulation frequency due to time-step choice, there's a noticeable trend of increasing frequencies with rising unload rates, albeit with a decrease in signal power. Analysing mid to low frequency power ratios indicates optimal unload rates likely fall within the lower to middle range tested. Simulations show potential to replicate impulsive AE source characteristics for short durations but require inclusion of damping effects from reflections for accurate long-term representation, crucial for evaluating multiple impulsive sources comprehensively.

6. References

- [1] S. Gholizadeh, Z. Leman, and B. Baharudin, "A review of the application of acoustic emission technique in engineering," *Struct.Eng.Mech*, vol. 54, no. 6, pp. 1075–1095, 2015.
- [2] Z. Yang, W. Yan, L. Jin, F. Li, and Z. Hou, "A novel feature representation method based on original waveforms for acoustic emission signals," *Mech Syst Signal Process*, vol. 135, p. 106365, 2020.

- [3] M. Motahari-Nezhad and S. M. Jafari, "Bearing remaining useful life prediction under starved lubricating condition using time domain acoustic emission signal processing," *Expert Syst Appl*, vol. 168, p. 114391, 2021.
- [4] E. Verstryngge, G. Lacidogna, F. Accornero, and A. Tomor, "A review on acoustic emission monitoring for damage detection in masonry structures," *Constr Build Mater*, vol. 268, p. 121089, 2021.
- [5] P. Kot, M. Muradov, M. Gkantou, G. S. Kamaris, K. Hashim, and D. Yeboah, "Recent advancements in non-destructive testing techniques for structural health monitoring," *Applied Sciences*, vol. 11, no. 6, p. 2750, 2021.
- [6] S. Hassani and U. Dackermann, "A Systematic Review of Advanced Sensor Technologies for Non-Destructive Testing and Structural Health Monitoring," *Sensors*, vol. 23, no. 4, p. 2204, 2023.
- [7] M. Carboni and D. Crivelli, "An acoustic emission based structural health monitoring approach to damage development in solid railway axles," *Int J Fatigue*, vol. 139, p. 105753, 2020.
- [8] M. G. Droubi, A. Stuart, J. Mowat, C. Noble, A. K. Prathuru, and N. H. Faisal, "Acoustic emission method to study fracture (Mode-I, II) and residual strength characteristics in composite-to-metal and metal-to-metal adhesively bonded joints," *J Adhes*, vol. 94, no. 5, pp. 347–386, 2018.
- [9] W. Nsengiyumva, S. Zhong, J. Lin, Q. Zhang, J. Zhong, and Y. Huang, "Advances, limitations and prospects of nondestructive testing and evaluation of thick composites and sandwich structures: A state-of-the-art review," *Compos Struct*, vol. 256, p. 112951, 2021.
- [10] M. Civera and C. Surace, "Non-destructive techniques for the condition and structural health monitoring of wind turbines: A literature review of the last 20 years," *Sensors*, vol. 22, no. 4, p. 1627, 2022.
- [11] M. G. R. Sause and M. A. Hamstad, "Numerical modeling of existing acoustic emission sensor absolute calibration approaches," *Sens Actuators A Phys*, vol. 269, pp. 294–307, 2018.
- [12] B. S. Wu and G. C. McLaskey, "Broadband calibration of acoustic emission and ultrasonic sensors from generalized ray theory and finite element models," *J Nondestr Eval*, vol. 37, no. 1, p. 8, 2018.
- [13] H. Vallen, "Proposal for an absolute AE sensor calibration setup," in *Advances in Acoustic Emission Technology: Proceedings of the World Conference on Acoustic Emission-2017*, Springer, 2019, pp. 9–24.
- [14] G. Shen, J. Zhang, and G. Lackner, "International acoustic emission standard analysis and development outlook," *Insight-Non-Destructive Testing and Condition Monitoring*, vol. 62, no. 12, pp. 724–734, 2020.
- [15] N. Ghadarah and D. Ayre, "A review on acoustic emission testing for structural health monitoring of polymer-based composites," *Sensors*, vol. 23, no. 15, p. 6945, 2023.
- [16] K. Ono, "Review on structural health evaluation with acoustic emission," *Applied Sciences*, vol. 8, no. 6, p. 958, 2018.
- [17] H. Khon and O. V. Bashkov, "The study of acoustic emission waves generated from different types of sources," *Mater Today Proc*, vol. 19, pp. 2243–2247, 2019.
- [18] D. F. Hesser, S. Mostafavi, G. K. Kocur, and B. Markert, "Identification of acoustic emission sources for structural health monitoring applications based on convolutional neural networks and deep transfer learning," *Neurocomputing*, vol. 453, pp. 1–12, 2021.
- [19] M. Dhuria, N. Grover, and K. Goyal, "Review of solution methodologies for structural analysis of composites," *European Journal of Mechanics-A/Solids*, p. 105157, 2023.
- [20] C. J. Abolle-Okoyeagu, J. P. Torralba, C. Yuhang, and R. L. Reuben, "Impact source identification on pipes using acoustic emission energy," *e-Journal of Nondestructive Testing*, vol. 28, no. 1, 2022.
- [21] T. Shiraiwa, M. Kawate, F. Briffod, T. Kasuya, and M. Enoki, "Evaluation of hydrogen-induced cracking in high-strength steel welded joints by acoustic emission technique," *Mater Des*, vol. 190, p. 108573, 2020.

- [22] Á. Angulo, H. Yang, J. Tang, A. Khadimallah, and S. Soua, “Structural Health Monitoring of Crack Initiation and Growth in Mooring Chains using FEA Methods for Acoustic Emission Characterisation.,” *Journal of Acoustic Emission*, vol. 36, 2019.
- [23] J. F. P. Moctezuma, “Characterization of damage evolution on metallic components using ultrasonic non-destructive methods,” 2019.
- [24] R. Joseph and V. Giurgiutiu, “Analytical and experimental study of fatigue-crack-growth ae signals in thin sheet metals,” *Sensors*, vol. 20, no. 20, p. 5835, 2020.
- [25] M. Smolnicki, G. Lesiuk, S. Duda, and A. M. P. de Jesus, “A review on finite-element simulation of fibre metal laminates,” *Archives of Computational Methods in Engineering*, vol. 30, no. 2, pp. 749–763, 2023.
- [26] W. Lu *et al.*, “FEM-based analysis on sensing out-of-plane displacements of low-order Lamb wave modes by CMUTs,” *J Appl Phys*, vol. 132, no. 20, 2022.
- [27] F. Bai, D. Gagar, P. Foote, and Y. Zhao, “Comparison of alternatives to amplitude thresholding for onset detection of acoustic emission signals,” *Mech Syst Signal Process*, vol. 84, pp. 717–730, 2017.
- [28] M. El-Shaib, R. Reuben, and T. Lim, “Predicting acoustic emission attenuation in small steel blocks using a ray tracing technique,” *Insight-Non-Destructive Testing and Condition Monitoring*, vol. 54, no. 12, pp. 673–680, 2012.
- [29] C. J. Abolle-Okoyeagu, “No title,” *Acoustic emission monitoring of pipes; combining finite element simulation and experiment for advanced source location and identification*, 2019.

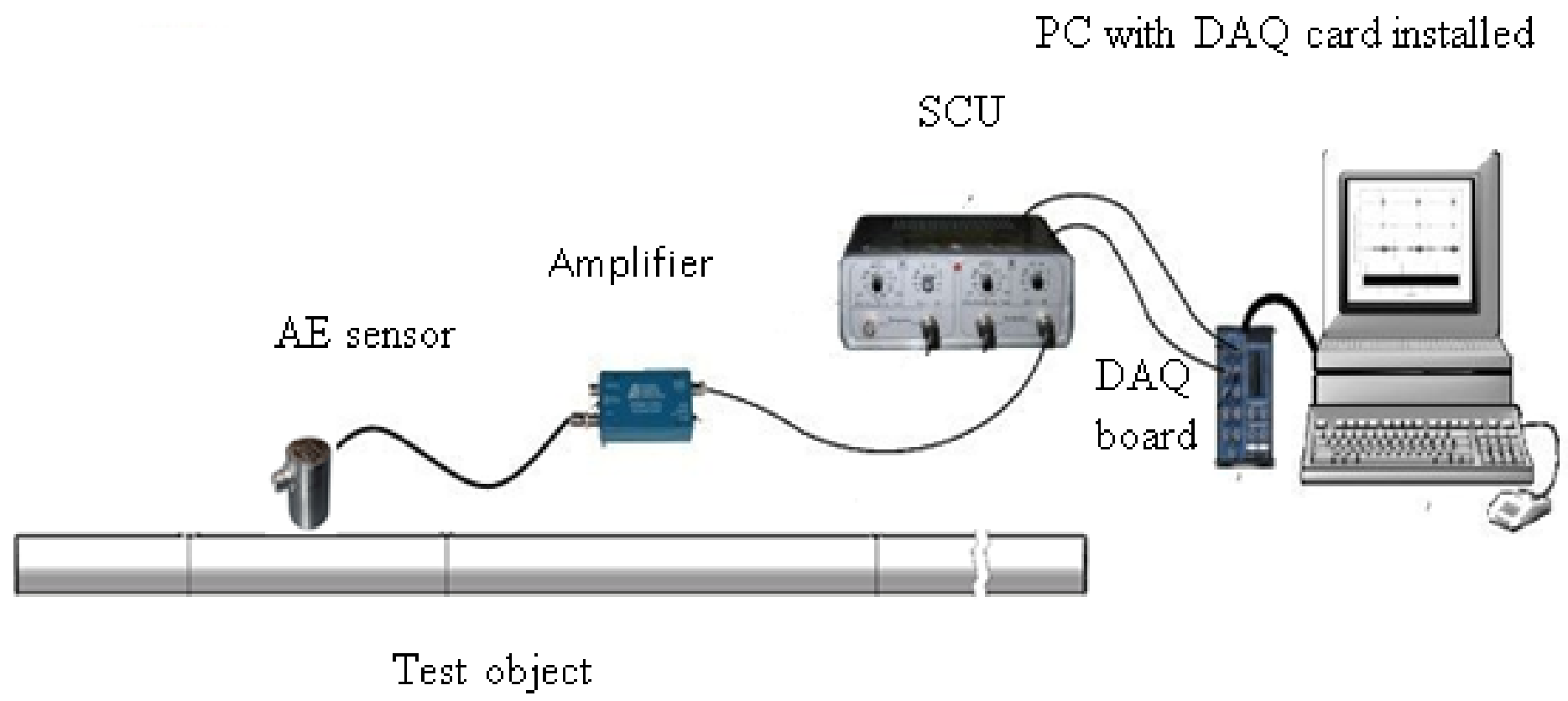
Quantitative Analysis of the Hsu-Nielsen Source through Advanced Measurement and Simulation Techniques

Robert Gordon University Aberdeen Scotland UK

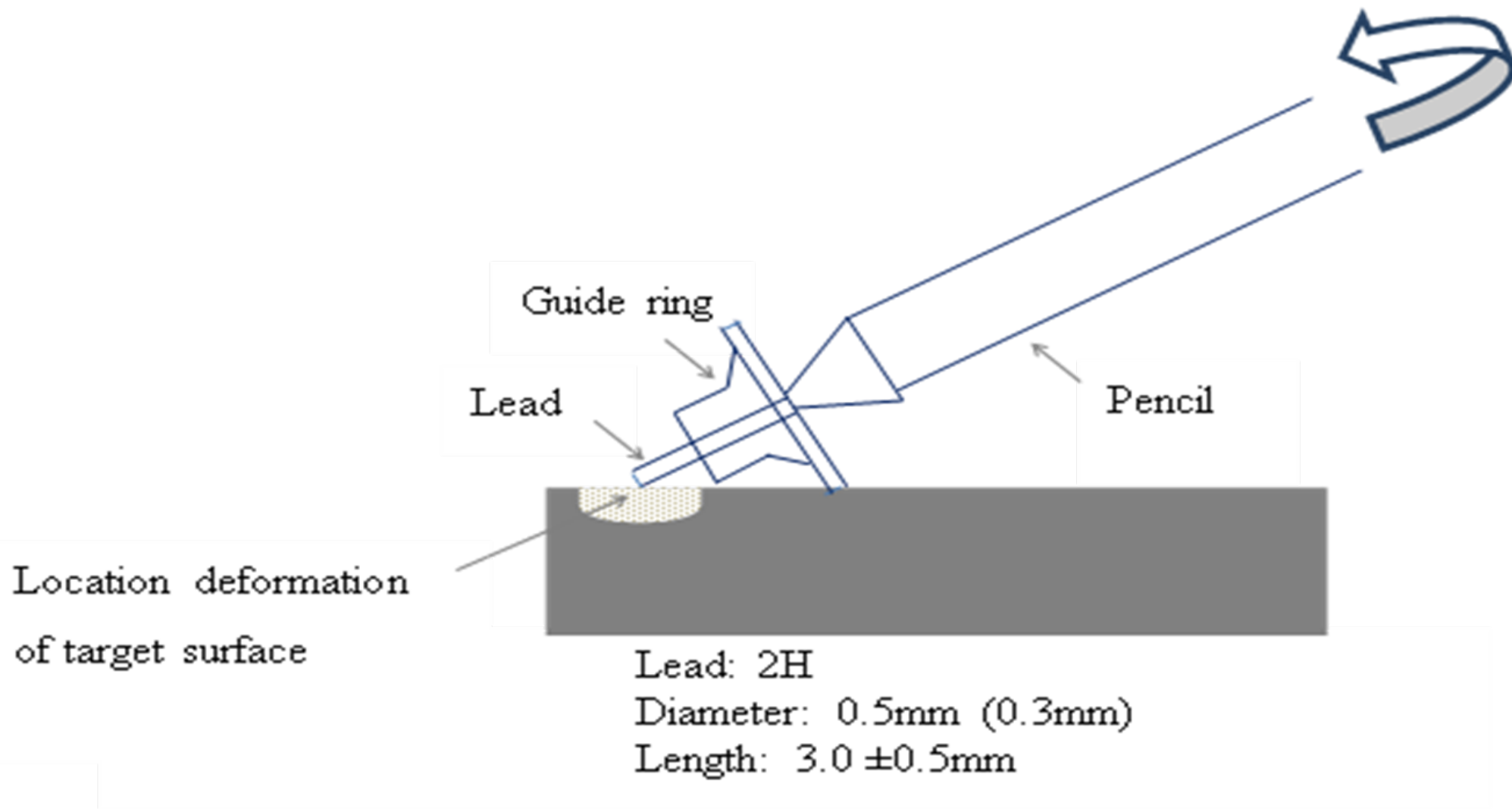
MA12208 - Dr Judith Abolle

Background

- Calibration of AE systems is essential for ensuring the accuracy and reliability of measurements which are critical for assessing the integrity and safety of various structures and materials.
- AE is a term used to describe high-frequency (0.1 to 1MHz) elastic stress waves generated by the rapid release of mechanical energy often associated with structural degradation.
- Finite Element Analysis (FEA) is a computational technique designed to predict and scrutinize the response of a structure subjected to various external forces.



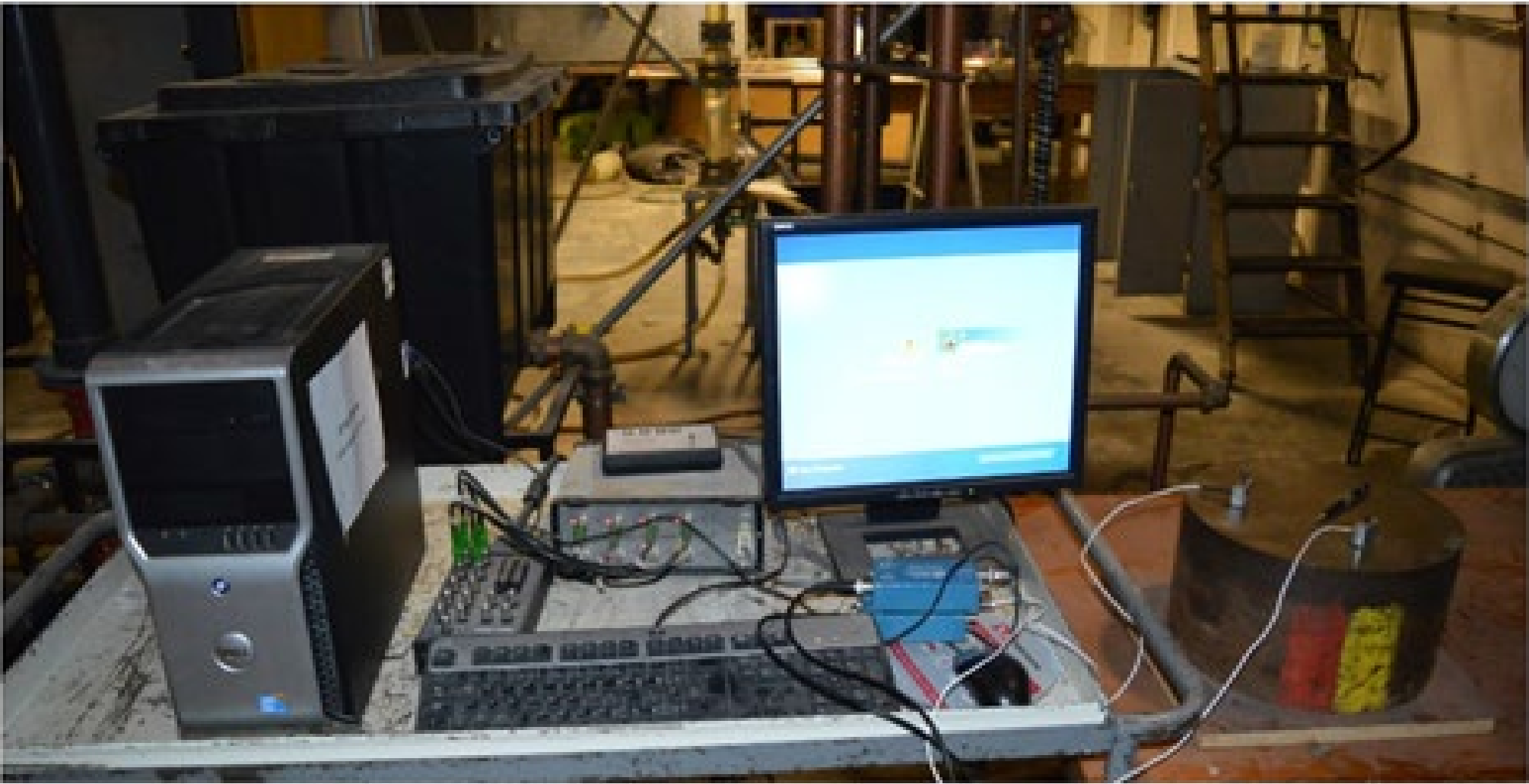
Schematic representation of a typical AE experimental system setup



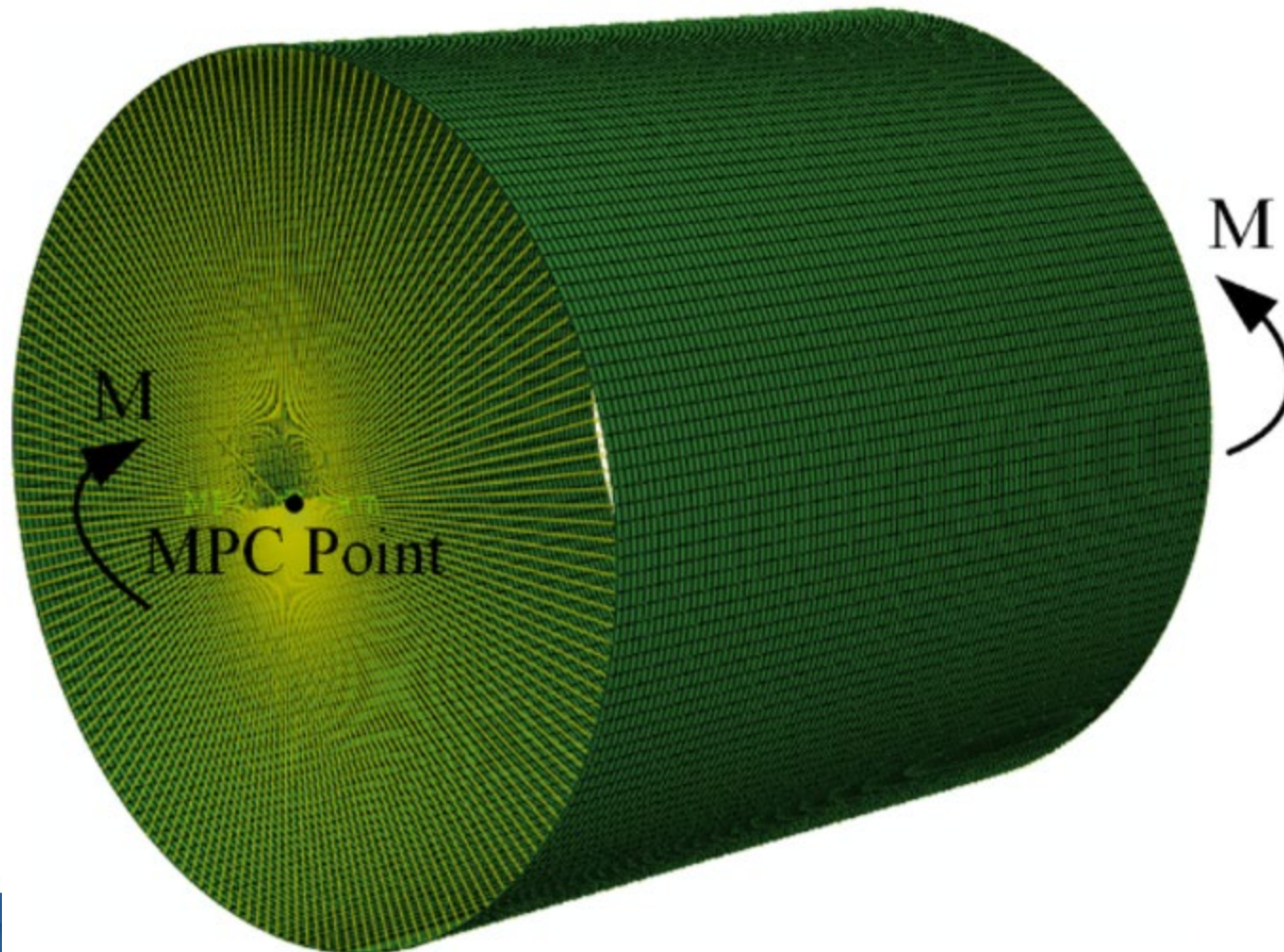
The Hsu Nielson Source



Experiments

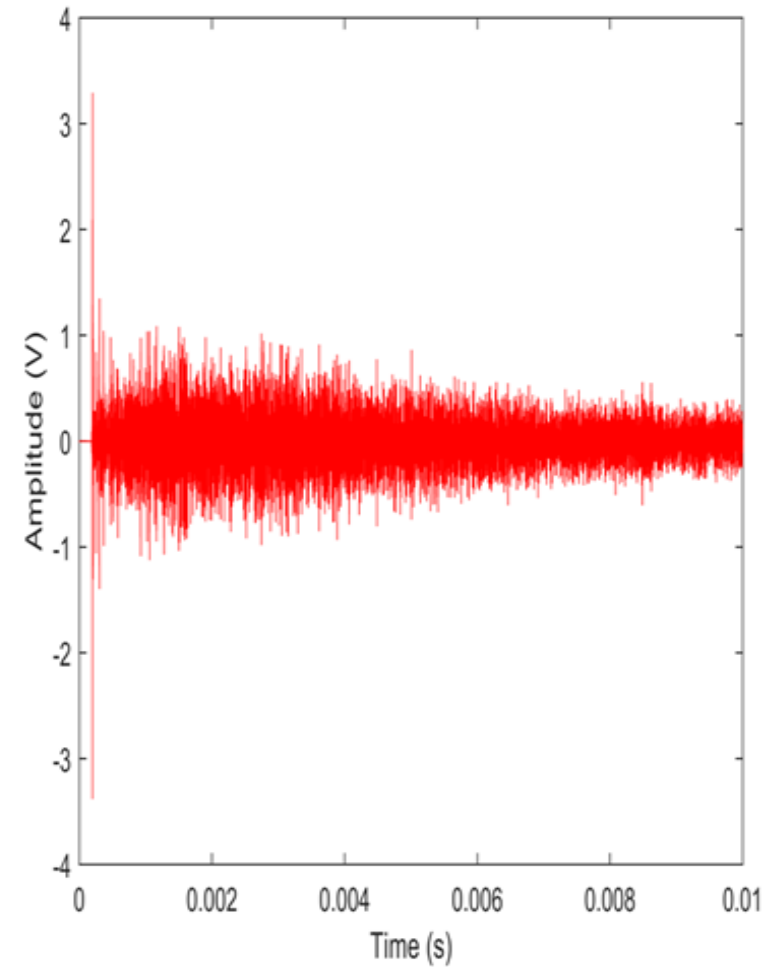
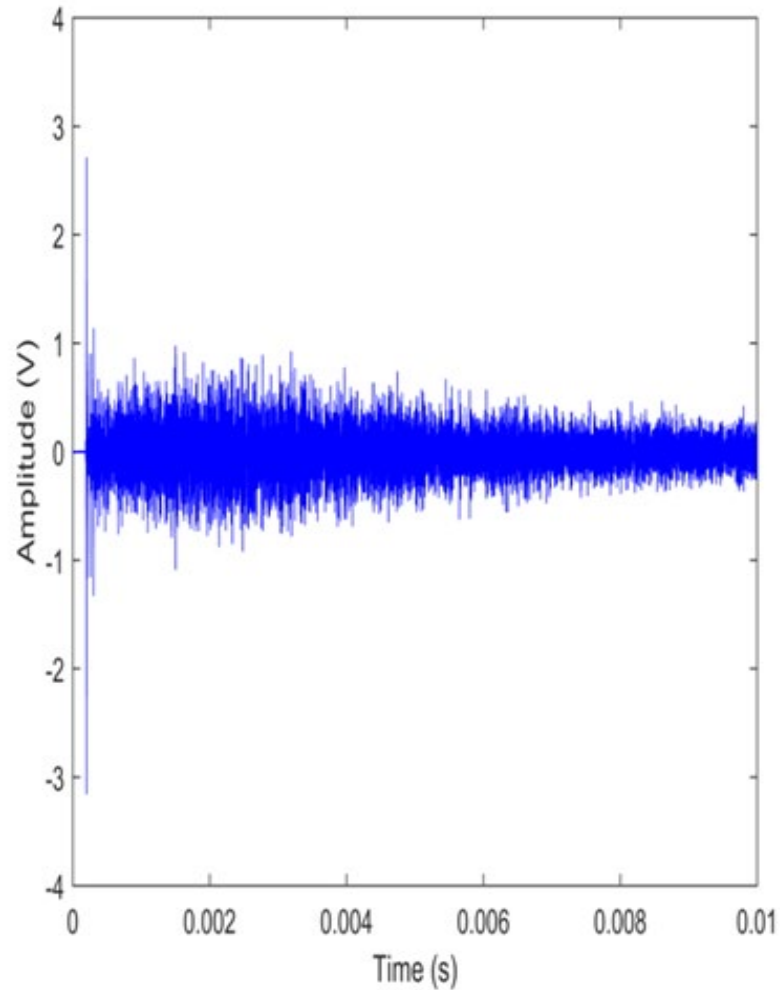


Simulation

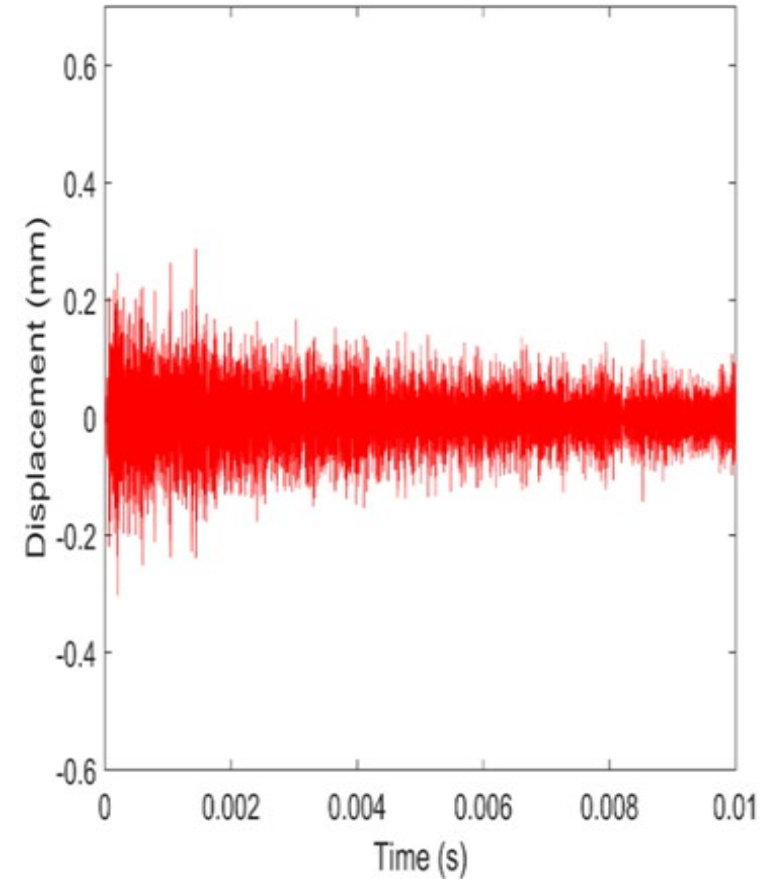
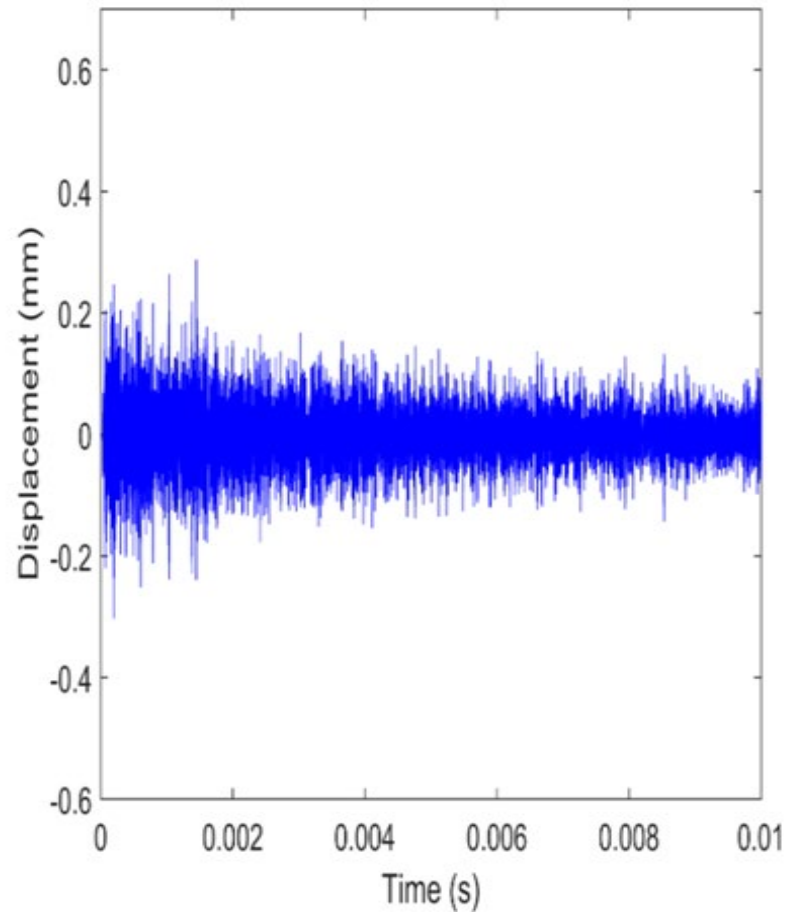


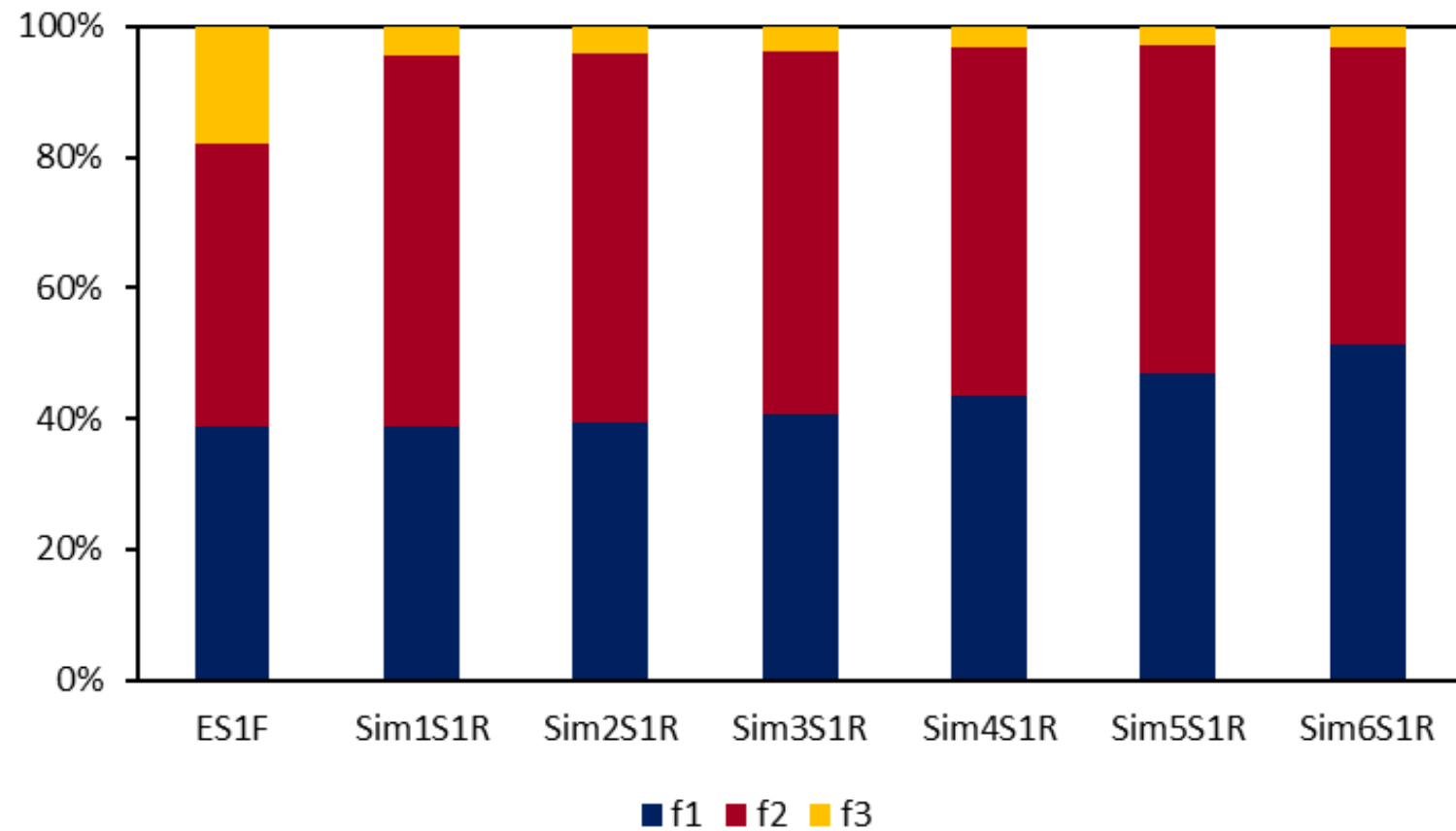


Experimental Results

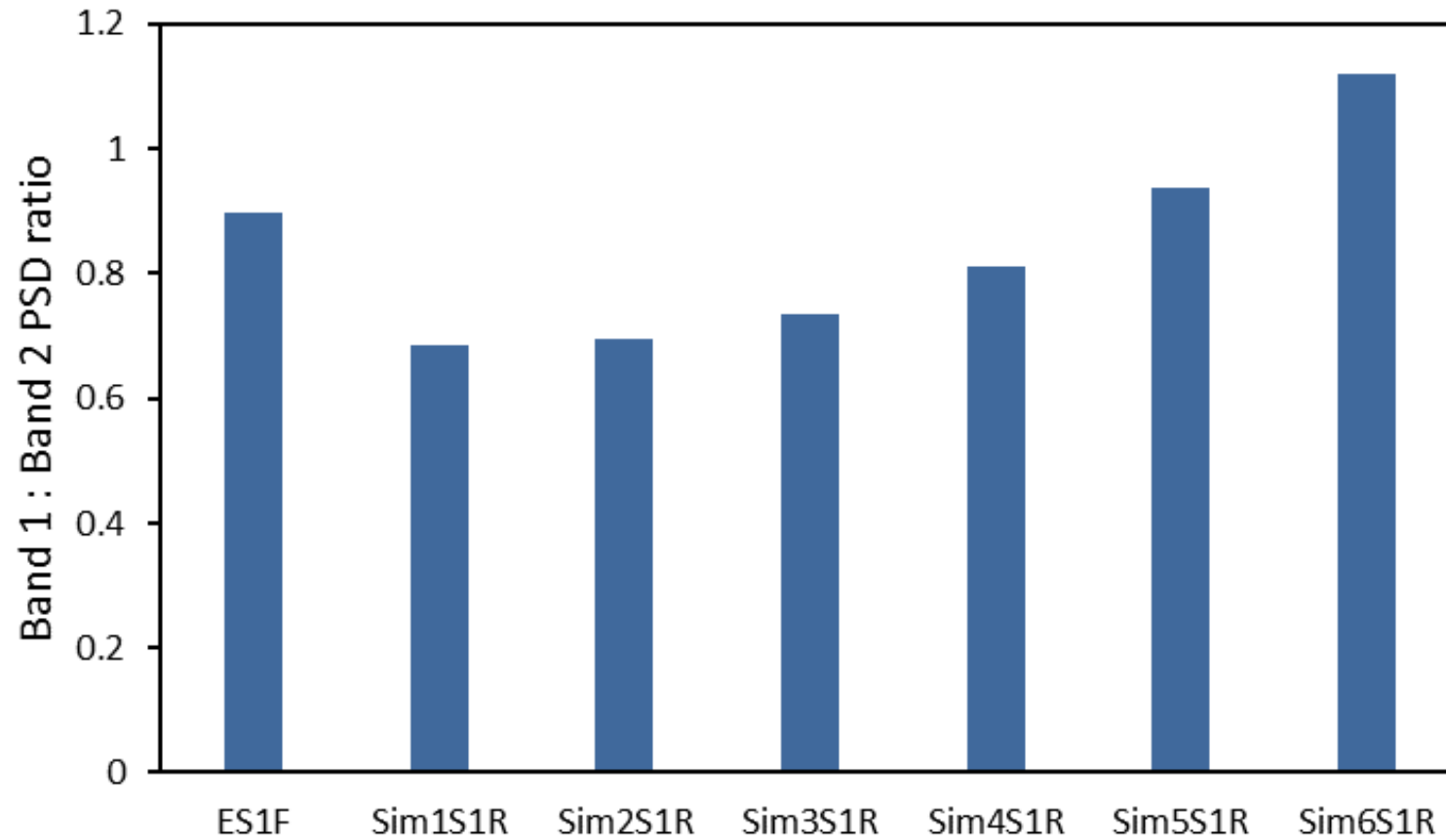


Simulation Results





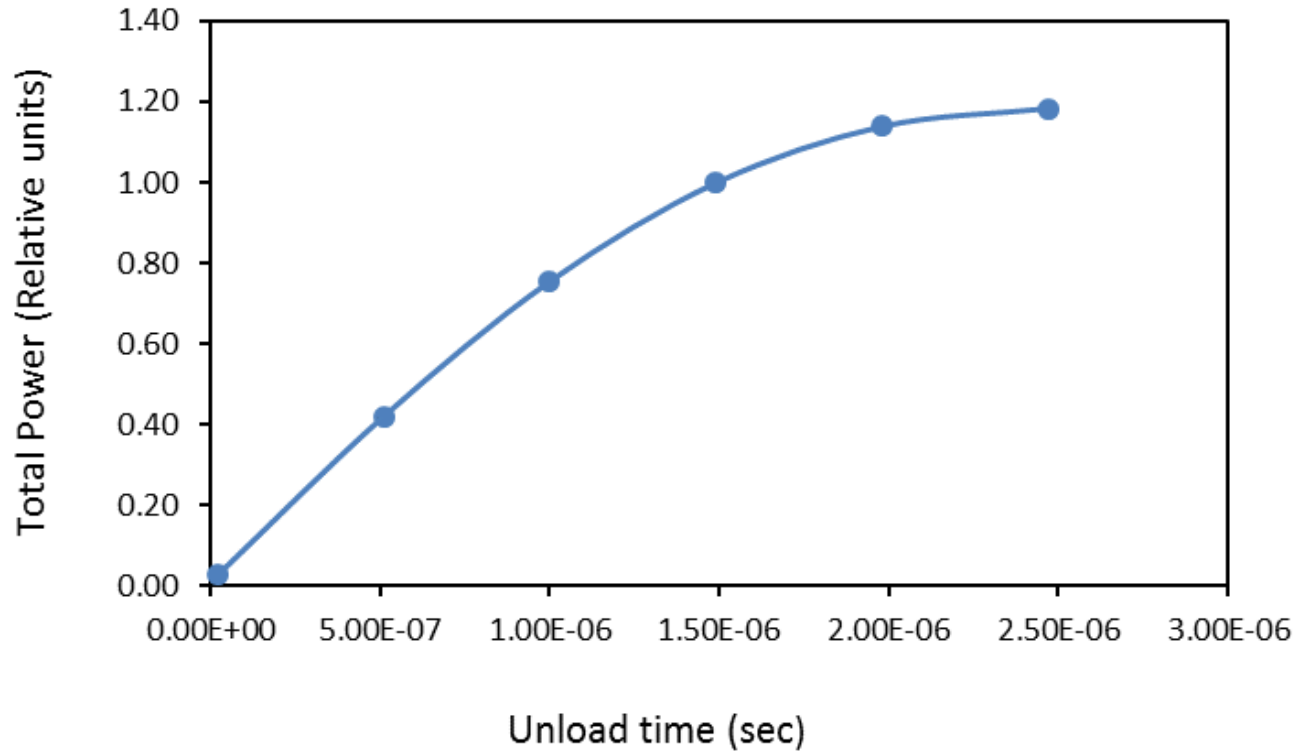
Comparison of experimental and simulated power content at the first sensor



Comparison of Experimental and simulated low frequency power ratio



Results



Power simulation vs unloading rate



Conclusion

- In the initial 25-30 μ s, the signals on the test object, both simulated and measured, display comparable characteristics.
- The simulation revealed that for short durations, it's possible to replicate the line structure of an impulsive AE source.
- Analysing and comparing the ratio of mid to low frequency power in both the simulated and measured signals suggests that the optimal unload rate is within the lower to middle range.
- Within the frequency domain, the simulations display an artificial cut-off near 400kHz, resulting from the chosen time-step.



Questions & Thank You